Design, Fabrication, Characterization and Simulation of AlN PMUT for Sonar Imaging Applications

Wenxing Chen , Shenglin Ma * , Xiaoyi Lai , Zhizhen Wang , Hui Zhao * , Qiang Zha , Yihsiang Chiu , Yufeng Jin

Posted Date: 21 May 2024

doi: 10.20944/preprints202405.1312.v1

Keywords: AlN PMUT; receiving sensitivity; acoustic characteristics simulation model

Article

Design, Fabrication, Characterization and Simulation of AlN PMUT for Sonar Imaging Applications

Wenxing Chen [1], Shenglin Ma [1,*], Xiaoyi Lai [1], Zhizhen Wang [1], Hui Zhao [2,*], Qiang Zha [3], Yihsiang Chiu [4] and Yufeng Jin [4]

[1] Department of Mechanical & Electrical Engineering, Xiamen University, Xiamen 361005, China
[2] Shanghai Marine Electronic Equipment Research Institute, Shanghai 201108, China
[3] Key Laboratory of Nanodevices and Applications Suzhou Institute of Nano-tech and Nano-bionics Chinese Academy of Sciences Suzhou, Jiangsu 215123, China
[4] School of Electronic and Computer Engineering, Peking University Shenzhen Graduate School, Shenzhen 518055, China
* Correspondence: mashenglin@xmu.edu.cn; zhaohui0094@163.com

Abstract: To address the requirements of sonar imaging, such as high receiving sensitivity, wide bandwidth, wide receiving angle, an AlN PMUT with an optimized ratio of 0.6 for the piezoelectric layer diameter to backside cavity diameter is proposed in this paper. A sample AlN PMUT is designed and fabricated with SOI substrate-based bulk MEMS process. The characterization test result of the sample demonstrates a -6 dB bandwidth of approximately 500 kHz and a measured receiving sensitivity per unit area of at 1.37 V/μPa/mm^2, which significantly surpasses the performance of previously reported PMUTs. The -6 dB horizontal angles of the AlN PMUT at 300 kHz and 500 kHz are measured 68.30° and 54.24°, respectively. To achieve an accurate prediction of its characteristics when being packaged and assembled in a receive array, numerical simulations with the consideration of film stress are conducted. The numerical result shows a maximum deviation of ±7% in the underwater receiving sensitivity across the frequency range of 200 kHz to 1000 kHz and a deviation of about 0.33% in the peak of underwater receiving sensitivity comparing to the experimental data. By such good agreement, the simulation method reveals its capability of providing theoretical foundation for enhancing the uniformity of the AlN PMUTs in future studies.

Keywords: AlN PMUT; receiving sensitivity; acoustic characteristics simulation model

1. Introduction

Ultrasonic transducer plays an important role in sonar imaging system of realizing the mutual conversion of electrical and acoustic signals. For sonar imaging equipment, ultrasonic transducers are usually fabricated with bulk Piezoceramics and work at their thickness vibration mode[1]. Although this kind of ultrasonic transducers have a long history and are developed as an industry with a high technological maturity, there are some limitations. For example, it features in the large volume size, high power consumption, requirements on precision machining and assembly, a high acoustic impedance with requirements on an additional acoustic impedance matching layer[2]. In addition, the resonant frequency of the ultrasonic transducer work at the thickness mode increases as the thickness of the piezoelectric material decreases, which means the rising of difficulty in machining and assemble to achieve high resonant frequency. For example, for resonant frequency of 500 kHz, the thickness of the piezoelectric material should be reduced to less than 3 mm. With the rapid development of micro-electro-mechanical systems (MEMS) technology, micro-ultrasonic transducers (MUTs) emerge to boom. While MUTs are featuring in small size, batch mode production, CMOS process compatibility, easiness of being arrayed with advanced package technology, many researchers have contributed to the exploration of its applications to replace the traditional ultrasonic transducers. According to the principle of operation, micro-ultrasonic transducers can be classified into two types: capacitive micro-ultrasonic transducer (CMUT), and piezoelectric micro-ultrasonic transducer (PMUT) [3-5]. Compared to CMUTs, PMUTs have the advantages of a wide resonant frequency range coverage and independence on DC bias voltage [6,7]. , Yang D [8] et al. proposed a piezoelectric AlN PMUT with a resonance frequency of 986 kHz, achieving an underwater receiving

 doi:10.20944/preprints202405.1312.v1

sensitivity of -178 dB (re: 1 V/μPa). For exploring the application of underwater imaging ,Yao, Y [1] et al. proposed a PMUTs which exhibits a transmit sensitivity of 146.59 dB (re: 1 μPa/V) and a receive sensitivity of −173.70 dB. For exploring application of underwater acoustic communication, Zhao, J [9] et al. proposed a transducer fabricated from piezoelectric ceramic with a maximum transmit voltage response of 152.1 dB (re: 1 μPa·m/V) and a receiving sensitivity of 182.5 dB. Reviewing the published literatures, it can be concluded that although the transmit sensitivity of AlN PMUT is much lower than that of traditional bulk transducers, their underwater receiving sensitivities are comparable. In addition, comparing with PZT, AlN is free of toxic lead and compatible with CMOS technology. Although its piezoelectric coefficient is one order of magnitude smaller than PZT, its dielectric constant is two orders of magnitude smaller, and theoretically the receiving sensitivity of AlN PMUT is one order of magnitude higher than that of PZT PMUT[6]. Therefore, a good promise is anticipated with AlN PMUT to replace bulk transducers in sonar imaging receiver arrays.

For a sonar imaging equipment, tens thousands channels of transducer is desired in receiver array. This imposed high demand on not only the receiver sensitivity, bandwidth, and receiving angle, but also the uniformity across all transducers to ensure the overall performance. However, AlN PMUTs based on MEMS process is sensitive to stress due to their inherent characteristics resulting from the suspended structure made of multi-layered thin films. Residual stress in AlN film still poses a significant challenge [10]. Additionally, considering subsequent steps during its package and assembly, different functional materials such as acoustic matching material and water sealing being used, the difficulty in stress control and design of PMUT further increases. In order to mitigate the influence of residual stress, novel structures are proposed, such as the PMUTs with V-shaped springs by Chen, X et al. [11] ,the tapered cantilever cluster PMUT by Gong, Y et al. [12], although both structures are more suitable for application in air. M Olfatnia et al. [13] and Firas Sammoura et al. [14] have investigated the influence of residual stress on the vibration behavior characteristics and displacement sensitivity of PZT piezoelectric thin films. In 2020, Glenn Ross et al. [15] used X-ray diffraction (XRD) technology to measure the residual stress in PMUTs at different positions on wafers. The results showed compressive stress ranges from -357 MPa to -56 MPa radially on the wafer and results in the shift in the first-order resonance frequency from 400 kHz to 600 kHz. The influence brought by residual stress is too significant to be neglected, therefore, simulation method factoring in the effects of stress on the characteristics of PMUTs should be developed to make a high precision prediction of the performance of PMUTS working in sonar receiver array.

In this paper, aiming at sonar imaging, an AlN PMUT is designed, fabricated, tested, a simulation method is established to achieve the high precision prediction of performance parameters such as operating frequency, receiving sensitivity, and bandwidth underwater.

2. Design of AlN PMUT

A 3D model of the PMUT with a cavity diameter of 350 μm is established as shown in Figure 1. The material parameters and dimensions of each layer are shown in Table 1. In Figure 2a, it can be seen that the circular piezoelectric film shows a very obvious zero-potential ring (white) when the ratio of the piezoelectric layer diameter (R1) to the cavity diameter (R2) is 1.1. The zero-potential ring is about 60% of the diameter of the film, while opposite potentials are inside and outside of the circle, respectively. Based on the distribution of the potential on the PMUT, in order to achieve better device performance, many scholars [14,16,17] proposed optimized sizes of upper electrode, which was usually designed to be 0.6-0.7 of the cavity's diameter. However, due to the fact that the size of the piezoelectric layer is larger than the radius of the cavity, the constraints of the piezoelectric layer are solidly supported constraints all around, which leads to a large anchor loss in the piezoelectric film. In order to reduce the anchor loss, the piezoelectric layer size is optimally designed When the ratio of the piezoelectric layer diameter (R1) to the cavity diameter (R2) is 0.6, the potential distributions of its piezoelectric film are all positive, as shown in Figure 2b, which indicates that the minimized anchor loss is achieved without decreasing the PMUT potential.

Table 1. Material parameters and dimensions of each layer.

Materials	Density (kg/m^3)	Poisson's ratio	Young's modulus (GPa)	Thickness (μm)

 doi:10.20944/preprints202405.1312.v1

Si	2330	0.28	170	3
Mo	10200	0.31	314	0.2
AlN	3600	0.24	340	2
SiO_2	2200	0.17	60	1

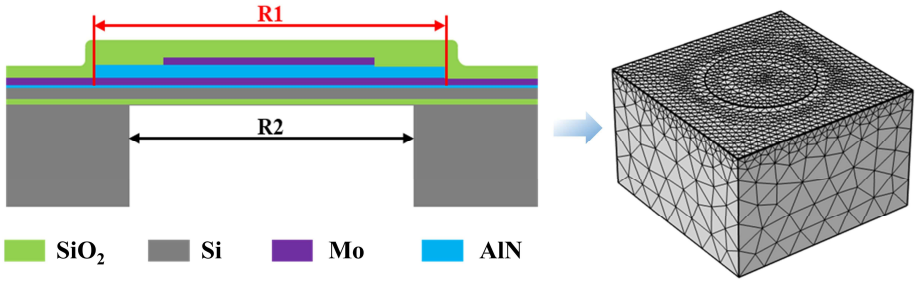

Figure 1. Schematic of PMUT cross-section and simulation model.

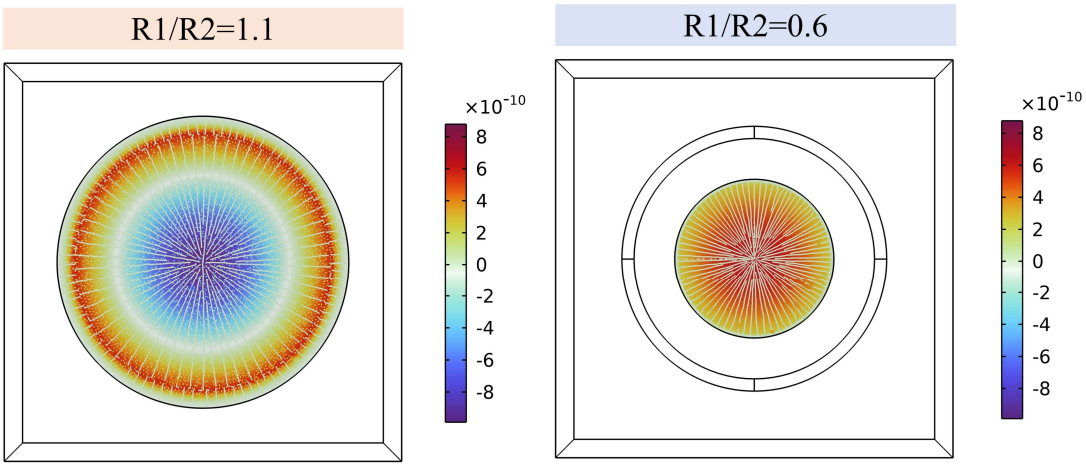

Figure 2. Potential simulation results of PMUT with different piezoelectric dimensions, they should be listed as: (**a**) R1:R2=1.1; (**b**) R1:R2=0.6.

In order to evaluate the effect of different residual stresses on the initial deflection of the PMUT, a steady state simulation is performed. The ratio of the diameter of the piezoelectric layer to the cavity's diameter is 0.6, a fixed constraint is set on the bottom silicon substrate, the residual stress of the AlN piezoelectric layer is set from -100 MPa to 500 MPa with step size of 100 MPa, the simulation results of the deflection in the direction of the Z-axis at the centre of the PMUT film are shown in Figure 3. Under the condition that the residual stress of the AlN piezoelectric layer is tensile stress (> 0 MPa), the film is deformed in a downward depression, the deflection of the film increases as the residual tensile stress increases. While under the condition that the residual stress of the AlN piezoelectric layer is compressive stress (< 0 MPa), the film is convex upward, the compressive stress causes the film to be in the yielding state, which is prone to lead to the film breaking and other situations.

Preprints.org (www.preprints.org) | NOT PEER-REVIEWED | Posted: 21 May 2024 doi:10.20944/preprints202405.1312.v1

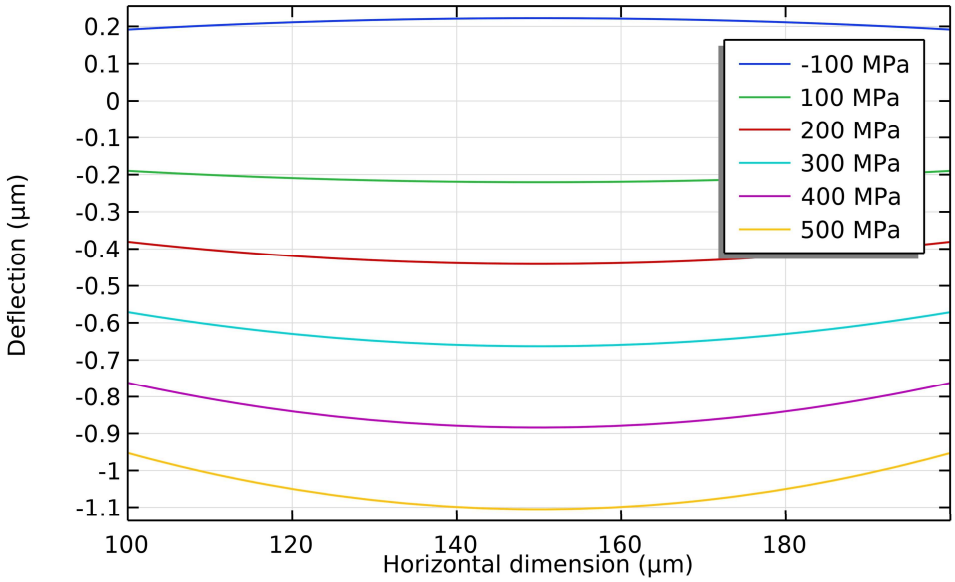

Figure 3. Simulation results of deflection of suspended stacked film at the centre with AlN piezoelectric layer under different residual stress conditions.

In order to evaluate the effect of different residual stresses on the resonance frequency of the PMUT, the residual stresses of the AlN piezoelectric layer are set to be from 100 MPa to 500 MPa (with step size of 100 MPa), the frequency sweep range is from 750 kHz to 780 kHz (with step size of 0.1 kHz), the displacement of the centre of the PMUT film in the Z-direction is shown in Figure 4. As the residual tensile stress of the AlN piezoelectric layer increases, the resonance frequency of the PMUT increases. The resonance frequency of the PMUT is 770.4 kHz when the residual tensile stress in the AlN piezoelectric layer is 500 MPa.

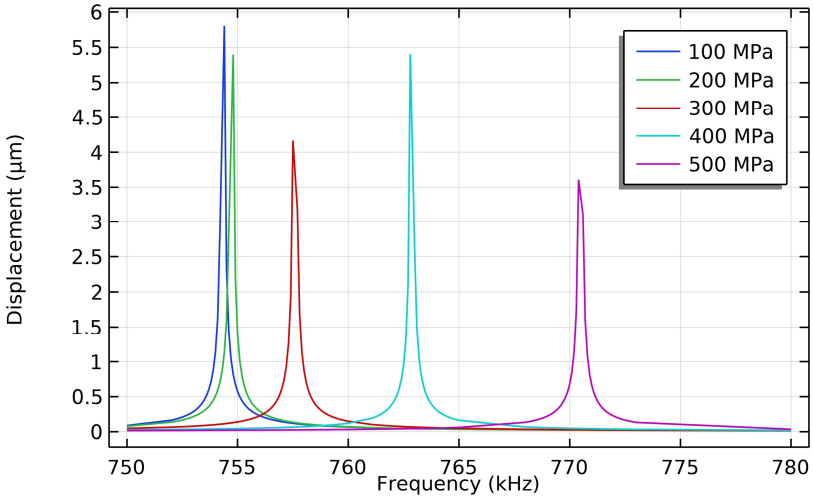

Figure 4. Resonance frequency simulation results of PMUT with AlN piezoelectric layer under different residual stress conditions.

3. Fabrication of AlN PMUT

The fabrication processes are schematically shown in Figure 5. An 8-inch high resistivity SOI wafer was chosen as the substrate to fabricate the AlN PMUTs, consisting of a Si device layer of 3 μm, a buried oxide layer of 1 μm, and a bulk silicon layer of 650 μm from top to bottom. Firstly, a sandwich structure of Mo/AlN/Mo is deposited on SOI wafer surface. Then, the top layer of Mo as electrode is patterned by ion beam etching (IBE). The AlN layer is patterned by inductively coupled plasma (ICP) etching. Next, a SiO_2 layer of 1 μm in thickness is deposited and patterned with RIE to expose both

 doi:10.20944/preprints202405.1312.v1

layers of Mo. After that, a Al layer of 1 μm in thickness is deposited to contact Mo by sputtering and patterned to form Pads by lift-off process. Finally, backside cavity beneath the sandwich structure of Mo/AlN/Mo is formed with Bosch process.

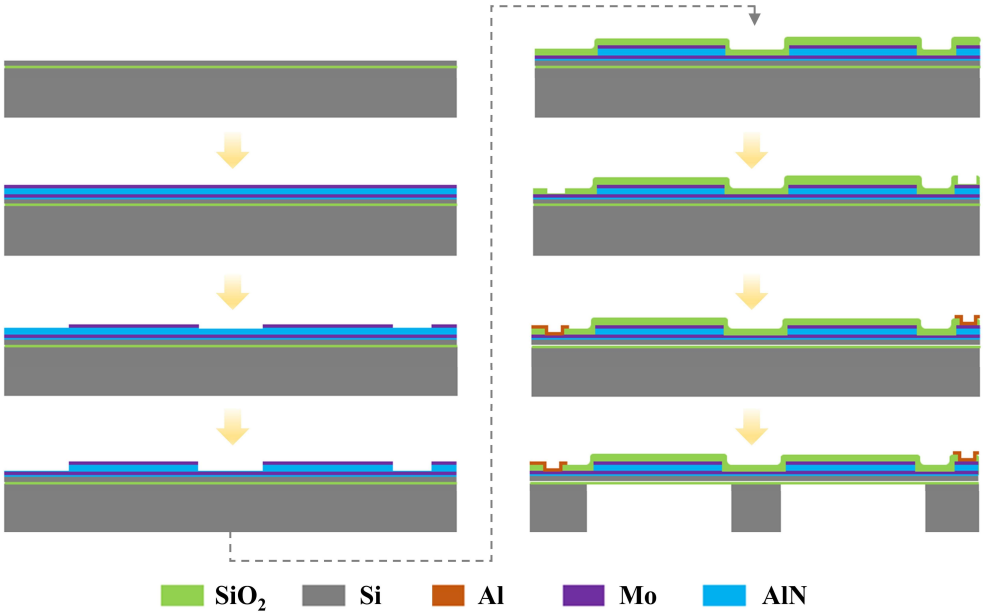

Figure 5. The process flow of PMUTs.

Figure 6 shows the cross-section of AlN PMUT. The measured thickness dimensions are listed as following, which are 1 μm for the silica insulating layer, 2 μm for the AlN, 1 μm for the buried oxygen layer, 3 μm for the device layer, 0.2 μm for the lower electrode, and 0.14 μm for the upper electrode. Figure 7a shows the picture of the circular array of 2 × 2 PMUTs, in which a total of four PMUTs are connected in parallel while each PMUT has the same structural dimensions. Figure 7b shows that the diameter of the PMUT back cavity is measured to be 345 μm.

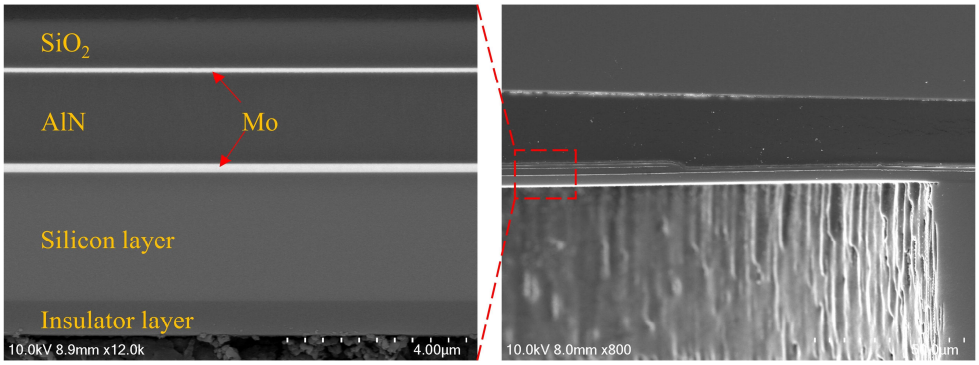

Figure 6. SEM image of PMUT cross-section.

Preprints.org (www.preprints.org) | NOT PEER-REVIEWED | Posted: 21 May 2024 doi:10.20944/preprints202405.1312.v1

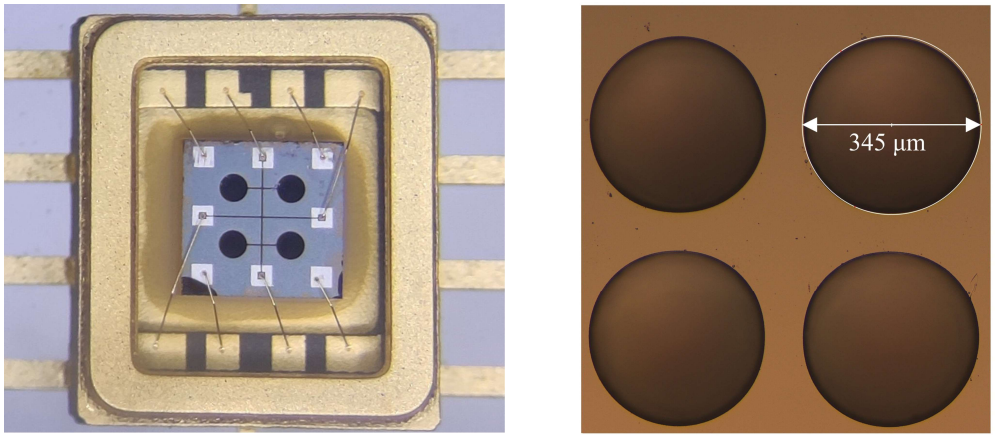

(**a**) (**b**)

Figure 7. (**a**) Optical microscope image of PMUTs; (**b**) Optical microscope image of the cavity.

4. The Characteristic Measurement of AlN PMUTs

4.1. Resonant Frequency Test

The resonant frequency of the PMUT in air was tested using an impedance analyzer (MICROTEST 6630) and the results are shown in Figure 8. The frequency setting was scanned from 600 kHz to 1 MHz, and the phase curve (red) peaked at 767.2 kHz, indicating that the first-order resonance frequency of the PMUT in air was 767.2 kHz. The impedance curve has a trough at 764 kHz with a resistance value of 9620 Ω and a peak at 773.6 kHz with a resistance value of 10,700 Ω.

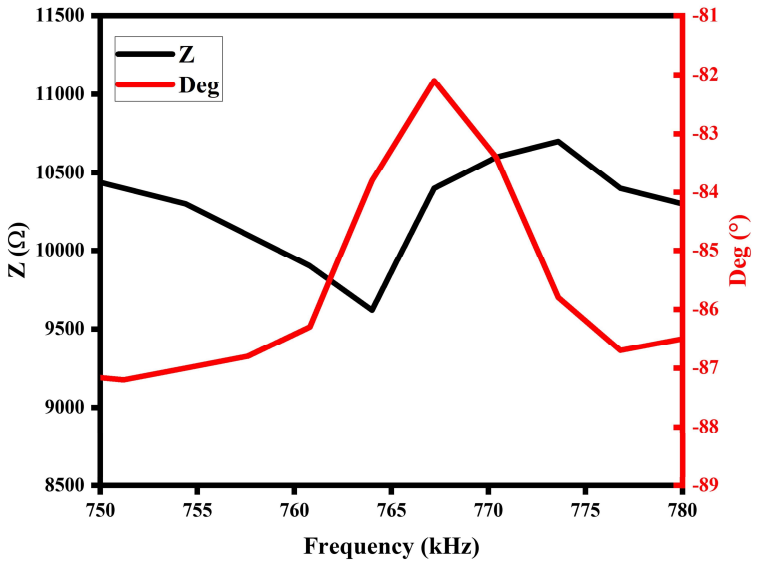

Figure 8. Measurements of the resonant frequency of PMUTs in air.

The deflection of the PMUT was measured using a VK-X1000 Shape Gauge and the test result is shown Figure 9. The deflection at the centre of the PMUT film was 1.19 μm and the film was deformed in a downward concave direction. Combining Figures 3 and 4, the deflection measurements match the deflection prediction for the 500 MPa stress case (1.1 μm) with an error of 0.09 μm, and the PMUT resonance frequency measurements also match the resonance frequency prediction for the 500 MPa stress case (770.4 kHz) with an error of 3.2 kHz, it can be derived that the PMUT film residual stress is 500 MPa.

 doi:10.20944/preprints202405.1312.v1

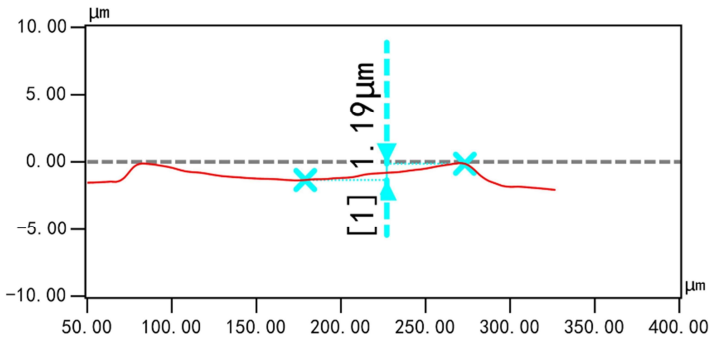

Figure 9. Measurement result of deflection at the centre of the film.

For evaluating the quality of ultrasonic transducers, electromechanical coupling coefficients are used to quantify such indicators, defined as:

$$k_{eff}{}^2 = \frac{f_p{}^2 - f_s{}^2}{f_p{}^2} \quad (1)$$

where f_s and f_p are the frequencies at the minimum and the maximum impedances, respectively. Therefore, the electrical coupling factor is calculated to be 2.47%.

4.2. Measurement of PMUT Underwater Acoustic Properties

In order to measure the underwater receiving sensitivity of the PMUTs, a commercial standard hydrophone from a research institute was used. At the same time, the PMUTs was used as a transmitter, and the standard hydrophone transducer and PMUT receiver were placed approximately 3.6 cm away from the transmitter to receive ultrasound. The signal generator outputs a 1 Vpp, 5-pulse sinusoidal signal, which is amplified 60 times by a power amplifier (Aigtek. ATA-2021B) to excite the PMUT transmitter to emit acoustic waves. The wave propagates through the water medium and is caught by the PMUT receiver as well as the surface of the hydrophone. The peak-to-peak values of the hydrophone and PMUT receiver voltages were read and analyzed on an oscilloscope. Figure 11 shows the receiving signal from the PMUT receiver with a peak voltage of 39.2 mV. The receiving sensitivity of the PMUT is calculated by:

$$S_R = S_{Hpp} + 20\lg\frac{V_R}{V_{Hpp}} \quad (2)$$

where S_{Hpp} is the sensitivity of the hydrophone, V_R is the voltage peak-to-peak value of the received signal of the PMUT, and V_{Hpp} is the voltage peak-to-peak value of the received signal of the hydrophone.

 doi:10.20944/preprints202405.1312.v1

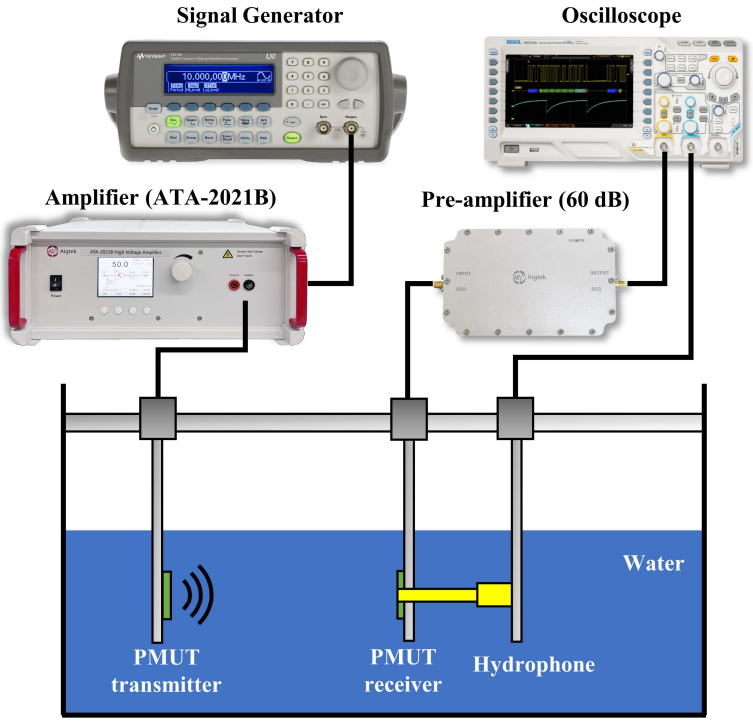

Figure 10. Schematic diagram of the test system for PMUT underwater receiving sensitivity.

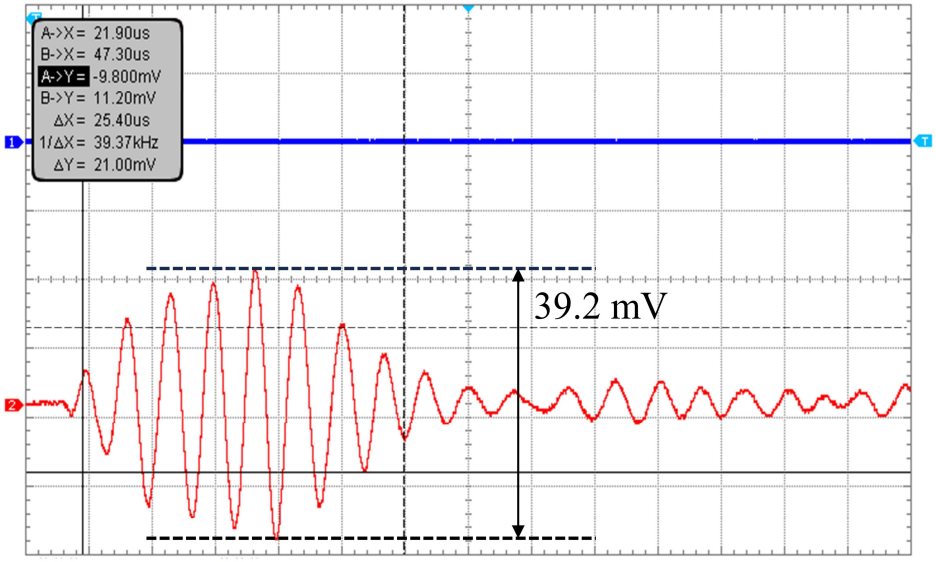

Figure 11. Measurement results of PMUT receiving signals.

4.3. Receiving Angle of PMUT

The receiving angle of PMUT can be generally divided into horizontal and vertical angles. The measurement principle of PMUT receiving angle is shown in Figure 12a. Pulse signals are generated by the signal generator generates output pulse signal, amplified by the power amplifier and stimulate the sound source to emit sound waves. Keeping the position and direction of the sound source transducer fixed, rotate the transducer in a certain step in the horizontal or vertical direction, record the peak-to-peak value of the output voltage of the transducer in different directions, then the receiving sensitivities of the transducer can be calculated according to the calibration data of the sound source. Based on the calculated sensitivities, receiving directivity diagrams in horizontal and

 doi:10.20944/preprints202405.1312.v1

vertical directions can be plotted. The PMUT in this paper is centre-symmetric, which means the horizontal and vertical angles can be considered to be basically equal.

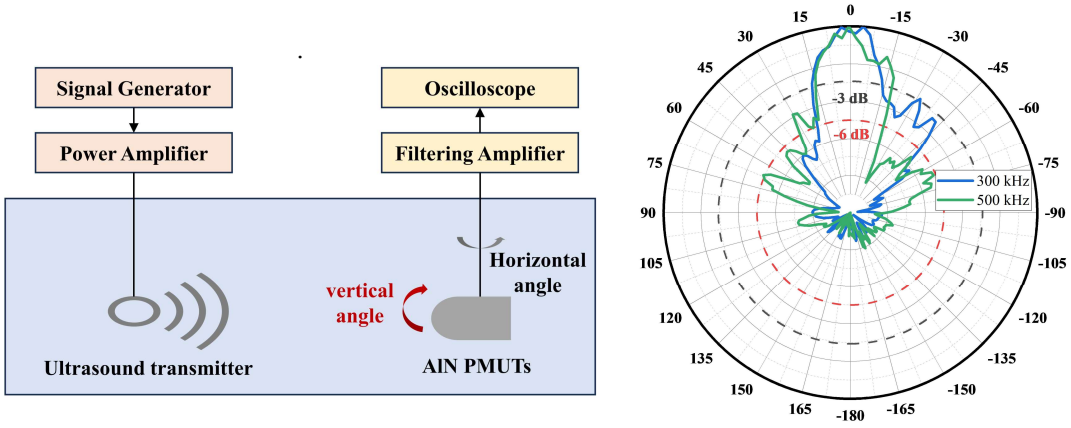

(**a**) (**b**)

Figure 12. (**a**) Schematic diagram of the measurement system for the receiving angle; (**b**) Measurements of the horizontal angle of the PMUTs.

The PMUTs after packaging was fixed on a rotatable fixture and submerged in water. The receiving angles of the PMUT at 300 kHz and 500 kHz were tested respectively, and the test results are shown in Figure 12b. According to the test results, it is observed that the PMUTs has a -3 dB horizontal angle of 31.45°, a -6 dB horizontal angle of 68.30° at 300 kHz, a -3 dB horizontal angle of 34.11° and a -6 dB horizontal angle of 54.24° at 500 kHz. The horizontal angle is improved by two orders of magnitude compared to conventional ultrasonic transducers applied in 3D mapping[18]

5. Simulation of PMUTs Underwater

The receiving sensitivity S_{rx} of a single PMUT is defined as[19]:

$$S_{rx} = \frac{V_{rx}}{P_{in}} = \frac{A_{eff}}{\eta} \frac{\eta^2 Z_{ele}}{\eta^2 Z_{ele} + Z_{tot}} \tag{3}$$

where Z_{ele} is the electrical impedance of a single PMUT and Z_{tot} is the sum of the mechanical and acoustic impedance of a single PMUT. When there are N PMUTs connected in parallel to form PMUTs, the receiving sensitivity S_{RX} of the PMUTs is:

$$S_{RX} = \frac{V_{RX}}{P_{in}} = \frac{NA_{eff}}{\eta} \frac{\eta^2 Z_{ele}/N}{\eta^2 Z_{ele}/N + Z_{tot}/N} \tag{4}$$

The receiving sensitivity of PMUTs is proportional to the number of parallel connections, which means that the receiving sensitivity can be improved by increasing the number of parallel connections of PMUT in a certain area and thus increasing the filling factor. During the subsequent acoustic characteristics simulations, once a single PMUT is simulated, the acoustic performance of the multiple PMUTs in parallel can be obtained by multiplying the multiplier on this basis.

The model for simulation of the acoustic characteristics of a single PMUT is shown in Figure 13, where the thickness of the PDMS is 0.5 mm, the diameter and the height of the cylindrical water domain are 6 mm and 36 mm, respectively. According to the measured results in Figures 8 and 9, the residual tensile stress of the AlN layer is set to be 500 MPa. To predict the acoustic characteristics of the PMUT, the frequency sweeping is performed from 200 kHz to 1 MHz in 100 kHz steps. As shown in Figure 14a, the sound pressure of the sound wave propagating to the surface of the PMUT is about 10.6 kPa. The received signals of the PMUT after 60 dB amplification at different frequencies are shown in Figure 14b. When the frequency is 600 kHz, the peak-to-peak voltage of the received signal after 60 dB amplification is about 5 V. The receiving sensitivity of a single PMUT is calculated to be -186.53 dB. Since the number of PMUTs is 4, the receiving sensitivity of the PMUTs at 600 kHz is -174.48 dB.

 doi:10.20944/preprints202405.1312.v1

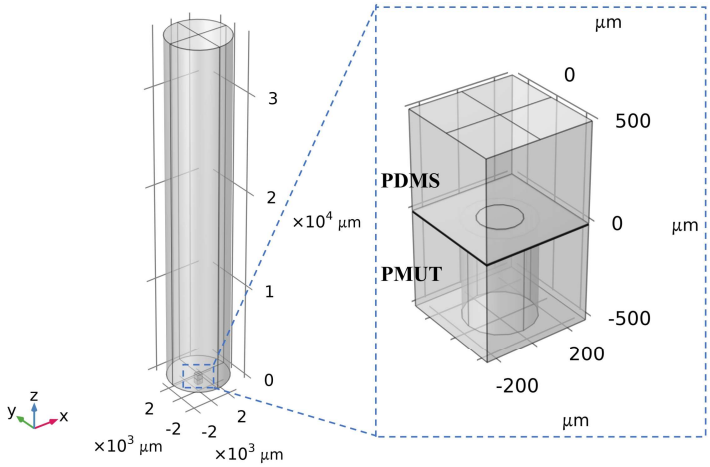

Figure 13. Simulation model of PMUT acoustic characteristics considering residual stress.

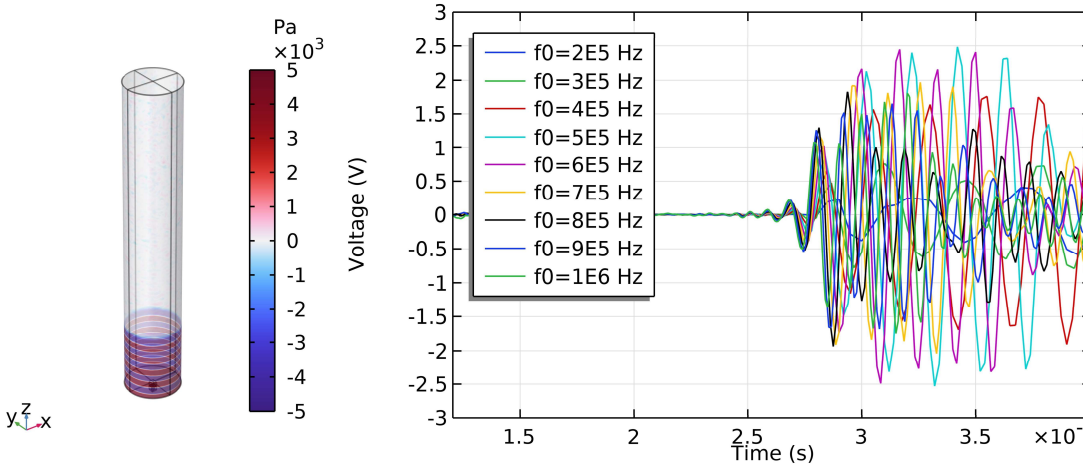

(**a**) (**b**)

Figure 14. PMUT acoustic receiving simulation results, (a) Sound pressure distribution; (b) Echo signals with frequencies from 200 kHz to 1000 kHz.

Figure 15a shows the curve of PMUT underwater receiving sensitivity against frequency. The optimum underwater receiving sensitivity obtained in simulations is -174.48 dB (600 kHz, amplified 60 dB), which shows only a small deviation of 0.33% comparing to the measured value -173.9 dB (600 kHz, amplified 60 dB). Figure 15b shows the relative error between the simulated and measured results of the receiving sensitivity of the PMUTs at different frequencies, where the maximum relative error is ±7%. The good agreement between simulation and measurement indicates that the PMUT simulation model can accurately predict the receiving sensitivity of the PMUT.

 doi:10.20944/preprints202405.1312.v1

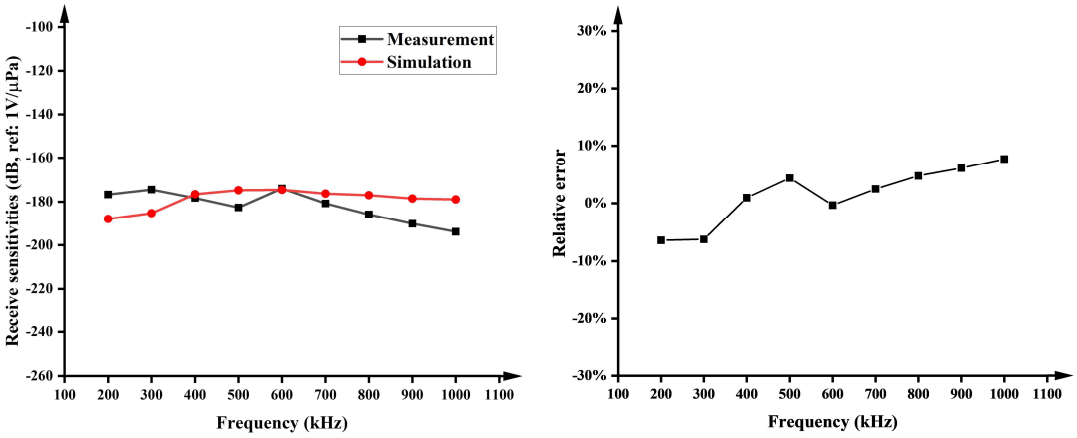

(**a**) (**b**)

Figure 15. Simulation and measurement results of PMUTs underwater receiving sensitivity (**a**) and relative error (**b**).

Table 2 compares PMUTs reported in recent years with resonant frequencies in the range of 400 kHz to 1 MHz. The -6 dB bandwidth of the PMUTs presented herein is about 500 kHz, which achieves a two-fold bandwidth enhancement at least. The receiver sensitivity per unit area after removing the amplifier's gain is 1.37 V/μPa/mm². Performance of the proposed PMUTs in this paper are superior to those of the currently reported PMUTs, with an improvement of nearly doubled.

Table 2. A comparison between the fabricated PMUTs presented in this paper and previously reported PMUTs in the literature is depicted.

Materials	UW[20]	ZJU[8]	WHU [1]	This work
Cavity size(μm)	460	280	500	345
Geometry	Square	circular	hexagonal	circular
Array	3×3	10×10	7×8	2×2
Resonant frequency (kHz, in air)	600	986	438.62	767.2
Piezoelectric material	AlN	AlN	$Sc_{0.2}Al_{0.8}N$	AlN
Receiving sensitivity(dB)	-237.39	-178	-173.4	-173.9
(Amplifier gain)	(0 dB)	(40 dB)	(40 dB)	(60 dB)
Receiving sensitivity per unit area (V/μPa/mm²)[1]	0.71	0.53	0.58	1.37
-6 dB bandwidth(kHz)	-	~1.5	~68	~500

[1] Without amplifier gain.

6. Conclusions

In this paper, a 2×2 AlN PMUTs with an optimized ratio of 0.6 for the piezoelectric layer diameter to backside cavity diameter is designed and fabricated for sonar imaging. The characterization test result of the sample demonstrates a -6 dB bandwidth of approximately 500 kHz and a measured receiving sensitivity per unit area of at 1.37 V/μPa/mm², which significantly surpasses the performance of previously reported PMUTs. Furthermore, a simulation model considering residual stress in the acoustic characteristics was established. The optimum underwater receiving sensitivity obtained in simulations is -174.48 dB (600 kHz), which shows only a small deviation of 0.33% comparing to the measured value -173.9 dB (600 kHz). Moreover, the relative error between simulated and measured underwater receiver sensitivities remains within ±7% across the frequency range of 200 kHz to 1000 kHz comparing to experimental data. This prove that the simulation is able to predict the underwater acoustic performance, providing a theoretical method for enhancing the uniformity of the AlN PMUTs in subsequent steps during package and assembly.

Author Contributions: Conceptualization, Shenglin Ma and Hui Zhao; methodology, Wenxing Chen, Xiaoyi Lai and Shenglin Ma; validation, Wenxing Chen, Xiaoyi Lai, Qiang Zha and Hui Zhao; formal analysis, Wenxing Chen; investigation, Wenxing Chen and Yihsiang Chiu; data curation, Wenxing Chen; writing—original draft preparation, Wenxing Chen; writing—review and editing, Shenglin Ma and Zhizhen Wang; supervision, Shenglin Ma and Yufeng Jin. All authors have read and agreed to the published version of the manuscript.

Funding: This research received no external funding.

Conflicts of Interest: The authors declare that they have no conflict of interest.

References

1. Yao, Y.; Jia, L.; Liu, C.; Wang, X.; Sun, C.; Liu, S.; Wu, G. A transceiver integrated piezoelectric micromachined ultrasound transducer array for underwater imaging. *Sensors and Actuators A: Physical* **2023**, *359*, doi:10.1016/j.sna.2023.114476.
2. Shuyu, L. *The principle and design of ultrasonic transducer*; Beijing: Science Press: 2004.
3. Roy, K.; Lee, J.E.-Y.; Lee, C. Thin-film PMUTs: a review of over 40 years of research. *Microsyst Nanoeng* **2023**, *9*, 95, doi:10.1038/s41378-023-00555-7.
4. Gong, D.; Ma, S.; Chiu, Y.; Lee, H.; Jin, Y. Study of the Properties of AlN PMUT used as a Wireless Power Receiver. *2019 IEEE 69th Electronic Components and Technology Conference (ECTC)* **2019**, 1503-1508.
5. Chiu, Y.; Wang, C.; Gong, D.; Li, N.; Ma, S.; Jin, Y. A Novel Ultrasonic TOF Ranging System Using AlN Based PMUTs. *Micromachines* **2021**, *12*, 284.
6. Lu, Y.; Tang, H.Y.; Fung, S.; Boser, B.E.; Horsley, D.A. Pulse-Echo Ultrasound Imaging Using an AlN Piezoelectric Micromachined Ultrasonic Transducer Array With Transmit Beam-Forming. *Journal of Microelectromechanical Systems* **2016**, *25*, 179-187, doi:10.1109/JMEMS.2015.2503336.
7. Hake, A.E.; Zhao, C.; Ping, L.; Grosh, K. Ultraminiature AlN diaphragm acoustic transducer. *Applied Physics Letters* **2020**, *117*, doi:10.1063/5.0020645.
8. Yang, D.; Yang, L.; Chen, X.; Qu, M.; Zhu, K.; Ding, H.; Li, D.; Bai, Y.; Ling, J.; Xu, J.; et al. A piezoelectric AlN MEMS hydrophone with high sensitivity and low noise density. *Sensors and Actuators A: Physical* **2021**, *318*, 112493, doi:https://doi.org/10.1016/j.sna.2020.112493.
9. Zhao, J.; Wang, H. Research on monometallic plate piezoelectric ceramic column array broadband high sensitivity transducer. *Applied Acoustics* **2023**, *205*, 109281, doi:https://doi.org/10.1016/j.apacoust.2023.109281.
10. Chen, W.L.; Yang, S.S.; Yuan, N.H.; Zhou, W.Y.; Yang, Y.P.; Lo, H.H.; Wang, P.J.; Lai, W.; Fuh, Y.k.; Li, T.T. Minimizing residual stress of aluminum nitride (AlN) thin films using multi-step deposition of DC pulsed sputtering. In Proceedings of the 2022 China Semiconductor Technology International Conference (CSTIC), 20-21 June 2022, 2022; pp. 1-4.
11. Chen, X.; Chen, D.; Liu, X.; Yang, D.; Pang, J.; Xie, J. Transmitting Sensitivity Enhancement of Piezoelectric Micromachined Ultrasonic Transducers via Residual Stress Localization by Stiffness Modification. *IEEE Electron Device Letters* **2019**, *40*, 796-799, doi:10.1109/LED.2019.2904293.
12. Gong, Y.; Zhang, M.L.; Sun, S.; Guo, W.L.; Sun, C.; Pang, W. Piezoelectric Micromachined Ultrasonic Transducers With Superior Frequency Control. *Journal of Microelectromechanical Systems* **2023**, *32*, 513-515, doi:10.1109/Jmems.2023.3305461.
13. Olfatnia, M.; Xu, T.; Ong, L.S.; Miao, J.M.; Wang, Z.H. Investigation of residual stress and its effects on the vibrational characteristics of piezoelectric-based multilayered microdiaphragms. *Journal of Micromechanics and Microengineering* **2009**, *20*, 015007.
14. Sammoura, F.; Smyth, K.; Kim, S.-G. Optimizing the electrode size of circular bimorph plates with different boundary conditions for maximum deflection of piezoelectric micromachined ultrasonic transducers. *Ultrasonics* **2013**, *53*, 328-334, doi:https://doi.org/10.1016/j.ultras.2012.06.015.
15. Ross, G.; Dong, H.Q.; Karuthedath, C.B.; Sebastian, A.T.; Pensala, T.; Paulasto-Kröckel, M. The impact of residual stress on resonating piezoelectric devices. *Mater Design* **2020**, *196*, doi:ARTN 10912610.1016/j.matdes.2020.109126.
16. Lu, Y.; Horsley, D.A. Modeling, Fabrication, and Characterization of Piezoelectric Micromachined Ultrasonic Transducer Arrays Based on Cavity SOI Wafers. *Journal of Microelectromechanical Systems* **2015**, *24*, 1142-1149, doi:10.1109/JMEMS.2014.2387154.
17. Cai, J.; Wang, Y.; Jiang, D.; Zhang, S.; Gu, Y.A.; Lou, L.; Gao, F.; Wu, T. Beyond fundamental resonance mode: high-order multi-band ALN PMUT for in vivo photoacoustic imaging. *Microsyst Nanoeng* **2022**, *8*, 116, doi:10.1038/s41378-022-00426-7.
18. Joe, H.; Cho, H.; Sung, M.; Kim, J.; Yu, S.-c. Sensor fusion of two sonar devices for underwater 3D mapping with an AUV. *Auton Robot* **2021**, *45*, 543-560, doi:10.1007/s10514-021-09986-5.
19. Jiang, X.; Lu, Y.; Tang, H.-Y.; Tsai, J.M.; Ng, E.J.; Daneman, M.J.; Boser, B.E.; Horsley, D.A. Monolithic ultrasound fingerprint sensor. *Microsyst Nanoeng* **2017**, *3*, 17059, doi:10.1038/micronano.2017.59.

 doi:10.20944/preprints202405.1312.v1

20. Wong, L.L.P.; Na, S.; Chen, A.I.; Li, Z.; Macecek, M.; Yeow, J.T.W. A feasibility study of piezoelectric micromachined ultrasonic transducers fabrication using a multi-user MEMS process. *Sensors and Actuators A: Physical* **2016**, *247*, 430-439, doi:https://doi.org/10.1016/j.sna.2016.06.029.